Theor. Comput. Fluid Dyn. (2009) 23:439–450
DOI 10.1007/s00162-009-0165-y

ORIGINAL ARTICLE

T. Lessinnes · F. Plunian · D. Carati

Helical shell models for MHD

Received: 10 December 2008 / Accepted: 9 June 2009 / Published online: 27 October 2009

Abstract A shell model for magnetohydrodynamics (MHD) is derived directly from the dynamical system driving the evolution of three helical modes interacting in a triad. The use of helical modes implies that two shell variables are required for the velocity as well as for the magnetic field. The advantage of the method is the automatic conservation of all the ideal quadratic MHD invariants. The number of coupling constants is however larger than in traditional shell models. This difficulty is worked around by introducing an averaging procedure that allows to derive the shell model coupling constants directly from the MHD equations. The resulting shell model is used to explore the influence of a helical forcing on the global properties of MHD turbulence close to the onset of the dynamo regime.

Keywords Turbulence modelling · MHD · Dynamo · Shell model · Helicity

PACS 47.65.-d · 47.27.E- · 47.27.Jv

1 Introduction

The analysis of turbulence has long been recognised as one of the most challenging problems of classical mechanics. Far away from the flow boundaries where a huge variety of geometry-dependent phenomena can be observed, turbulence in fluids is characterised by a single dimensionless parameter referred to as the Reynolds number $R_e = UL/\nu$. Here, U and L are the characteristic velocity and length of the flow, and ν is the viscosity of the fluid. Turbulence is observed for high values of this number, and both analytical theories and numerical simulations are very much limited in this range of parameters. In particular, for a three-dimensional turbulent flow, it is well known that the number of grid points required to capture all the turbulent scales increases like $R_e^{9/4}$, which makes the direct simulation of high R_e flow prohibitive [1].

For electro-conducting fluids and plasmas, the Navier–Stokes equation for the fluid velocity has to be supplemented by an equation for the magnetic field, leading to the magnetohydrodynamics (MHD) formalism. The situation of MHD turbulence is even more complex since a second dimensionless parameter has to be

Communicated by O. Zikanov

T. Lessinnes (✉) · D. Carati
Statistical and Plasma Physics, Université Libre de Bruxelles (ULB), Campus Plaine, CP 231, B-1050 Brussels, Belgium
E-mail: tlessinn@ulb.ac.be
D. Carati
E-mail: dcarati@ulb.ac.be
F. Plunian
Laboratoire de Géophysique Interne et Tectonophysique, Université Joseph Fourier, B.P. 53, 38041 Grenoble Cedex 9, France
E-mail: Franck.Plunian@ujf-grenoble.fr

introduced: the ratio between the viscosity ν and the magnetic diffusivity η. The so-called magnetic Prandtl number $P_\mathrm{m} = \nu/\eta$ may also be very large or very small depending on the fluid, characterising the fact that the viscous and Joule dissipations usually take place at very different characteristic scales. As a consequence, the simulation of MHD turbulence appears to be even more challenging.

Shell models have been introduced to work around these difficulties. First developed for fluid turbulence [2–6], they represent the entire velocity field by a limited number of interacting variables. In the Fourier representation of the velocity, all the modes with a wavelength l such that $l_1 \leq l < l_2$ are then replaced by one or two complex variables. These Fourier modes correspond to wave vectors that, in the Fourier space, belong to a shell defined as the domain between two spheres, which explains the terminology "shell model". The equations of evolution of the model's variables are, then, written in such a way that the Navier–Stokes ideal invariants—energy and kinetic helicity—are conserved by the nonlinear couplings in the model. This approach has been extended to MHD [7–11]. It correctly reproduces well-known properties of MHD flows: energy spectra as well as the spontaneous generation of the magnetic field (dynamo effect) in 3D simulations and the impossibility of such an effect in 2D turbulence. These models, making use of only one complex variable per shell, however, suffer from a very crude description of the helicity: in each shell, the helicity and the energy are not independent quantities.

In order to solve this difficulty, Benzi et al. [12] have introduced shell models for Navier–Stokes turbulence that use two complex variables per shell. This work was strongly motivated by a description of the velocity field in terms of eigenvectors of the curl operator [13]. It was shown that each three-dimensional velocity Fourier modes can be represented by a superposition of two eigenvectors corresponding, respectively, to maximal and minimal helicity. The models developed by Benzi et al. [12] identify the two complex variables per shell to the amplitude of these eigenvectors. Although these models propose a very elegant framework for representing helicity in shell models, they have the drawback to contain several free parameters. Indeed, the constraints imposed by the energy and the helicity conservation are too few to prescribe the amplitude of all the possible nonlinear couplings between the two variables per shell, even when only local interactions are considered.

The purpose of this work is threefold. First, the analysis of turbulence in terms of helical modes is extended to the MHD equation in Sect. 2. Since, the MHD equations conserve the magnetic helicity in the ideal limit, it appears relevant to express both the velocity and the magnetic fields in terms of helical modes. Second, the work of Benzi et al. [12] is also extended to MHD using a somewhat different approach. Shell models with a proper representation of both kinetic and magnetic helicities are derived in Sect. 3 as a direct translation of the triadic interactions that appear in the MHD equations into the shell model formalism. This approach automatically ensures that all the invariance properties of the original MHD equations are recovered in the MHD shell model. Third, the difficulty raised by the number of arbitrary free parameters in the shell model is worked around by introducing an averaging procedure to compute all the coupling constants. Indeed, the helical MHD shell models, like the helical Navier–Stokes models, contain several undetermined coupling constants. The averaging method presented in Sect. 3 leads to a shell model where only a freedom on the phases remains, at least, when only local interactions are considered in the nonlinearities. In Sect. 4, this helical shell model for MHD is numerically solved and the influence of the helicity injection rate due to the forcing is explored.

2 Helical decomposition of MHD equations

The incompressible MHD equations for the velocity $\mathbf{u}$ and magnetic $\mathbf{b}$ fields read:

$$\begin{aligned} \left(\tfrac{\partial}{\partial t} - \nu\nabla^2\right)\mathbf{u} &= -(\mathbf{u}\cdot\nabla)\,\mathbf{u} + (\mathbf{b}\cdot\nabla)\,\mathbf{b} - \nabla p + \mathbf{f}, & \nabla\cdot\mathbf{u} &= 0, \\ \left(\tfrac{\partial}{\partial t} - \eta\nabla^2\right)\mathbf{b} &= -(\mathbf{u}\cdot\nabla)\,\mathbf{b} + (\mathbf{b}\cdot\nabla)\,\mathbf{u}, & \nabla\cdot\mathbf{b} &= 0, \end{aligned} \tag{1}$$

where p is the total pressure and $\mathbf{f}$ is a forcing. The problem of homogeneous turbulence has been studied for decades by assuming periodic boundary conditions in a cubic box of length L and by using a Fourier representation of these equations. For incompressible Navier–Stokes equations ($\mathbf{b} = \mathbf{0}$), Waleffe [13] introduced a slightly different representation based on the eigenvectors $\mathbf{h}_s(\mathbf{k})$ of the curl operator:

$$i\mathbf{k}\times\mathbf{h}_s(\mathbf{k}) = s\,k\,\mathbf{h}_s(\mathbf{k}), \tag{2}$$

where $s = \pm 1$ and $k = ||\mathbf{k}||$. The product $\pm k$ represents the eigenvalue of the curl operator. It should be noted however that Eq. 2 defines the eigenvector $\mathbf{h}_s(\mathbf{k})$ up to an arbitrary rotation of axis $\mathbf{k}$. One particular choice has been proposed [13]. It is based on the introduction of an arbitrary vector $\mathbf{z}_\mathbf{k}$ that, in general, may depend on $\mathbf{k}$.

In particular, it cannot be proportional to $\mathbf{k}$. It is then easy to build a unit vector $\mathbf{u}_1(\mathbf{k}) = (\mathbf{z}_\mathbf{k} \times \mathbf{k})/||(\mathbf{z}_\mathbf{k} \times \mathbf{k})||$ that is perpendicular to $\mathbf{k}$. A second unit vector perpendicular to $\mathbf{k}$ is then given by $\mathbf{u}_2(\mathbf{k}) = \mathbf{u}_1(\mathbf{k}) \times \mathbf{k}/k$. In that case, the helical vectors can be written as

$$\mathbf{h}_s(\mathbf{k}) = \mathbf{u}_2(\mathbf{k}) + i\ s\ \mathbf{u}_1(\mathbf{k}). \tag{3}$$

The extension of this approach to the MHD equations is trivial and the velocity and magnetic fields can then be expanded in terms of helical modes rather that Fourier modes as follows:

$$\mathbf{u}(\mathbf{x}) = \sum_\mathbf{k} \left(u^+(\mathbf{k})\mathbf{h}_+(\mathbf{k}) + u^-(\mathbf{k})\ \mathbf{h}_-(\mathbf{k})\right) \mathrm{e}^{i\mathbf{kx}}, \tag{4}$$

$$\mathbf{b}(\mathbf{x}) = \sum_\mathbf{k} \left(b^+(\mathbf{k})\mathbf{h}_+(\mathbf{k}) + b^-(\mathbf{k})\ \mathbf{h}_-(\mathbf{k})\right) \mathrm{e}^{i\mathbf{kx}}. \tag{5}$$

Replacing the expressions (4–5) for $\mathbf{u}$ and $\mathbf{b}$ in Eq. 1 and projecting on $\mathbf{h}_{s_k}(\mathbf{k})$ ($s_k = \pm$) leads to the following dynamical system for the helical mode evolution:

$$\left(\frac{\partial}{\partial t} + \nu k^2\right) u^{s_k}(\mathbf{k}) = \frac{1}{2} \sum_{\mathbf{k}+\mathbf{p}+\mathbf{q}=0} \sum_{s_p,s_q} \left(s_p p - s_q q\right)\ g\ \left(u^{s_p}(\mathbf{p})u^{s_q}(\mathbf{q}) - b^{s_p}(\mathbf{p})b^{s_q}(\mathbf{q})\right)^* + f^{s_k}(\mathbf{k}), \tag{6}$$

$$\left(\frac{\partial}{\partial t} + \eta k^2\right) b^{s_k}(\mathbf{k}) = -\frac{1}{2} \sum_{\mathbf{k}+\mathbf{p}+\mathbf{q}=0} \sum_{s_p,s_q} s_k\, k\, g\, \left(u^{s_p}(\mathbf{p})b^{s_q}(\mathbf{q}) - b^{s_p}(\mathbf{p})u^{s_q}(\mathbf{q})\right)^*, \tag{7}$$

where g is a function of $\mathbf{k}$, $\mathbf{p}$, $\mathbf{q}$, s_k, s_p and s_q defined in [13] (up to a conventional factor 2) by

$$g(\mathbf{k}, \mathbf{p}, \mathbf{q}, s_k, s_p, s_q) \equiv -\frac{1}{\mathbf{h}_{s_k}(\mathbf{k})^* \cdot \mathbf{h}_{s_k}(\mathbf{k})} (\mathbf{h}_{s_k}(\mathbf{k})^* \times \mathbf{h}_{s_p}(\mathbf{p})^*) \cdot \mathbf{h}_{s_q}(\mathbf{q})^*. \tag{8}$$

Considering a single triadic interaction, it is actually not necessary to introduce an arbitrary unit vector $\mathbf{z}$ to define the unit vectors $\mathbf{u}_1$ and $\mathbf{u}_2$. Indeed, there is a natural direction which is represented by the unit vector perpendicular to the plane of the triad:

$$\boldsymbol{\lambda} = (\mathbf{k} \times \mathbf{p})/||\mathbf{k} \times \mathbf{p}|| = (\mathbf{p} \times \mathbf{q})/||\mathbf{p} \times \mathbf{q}|| = (\mathbf{q} \times \mathbf{k})/||\mathbf{q} \times \mathbf{k}||. \tag{9}$$

A second unit vector $\mu_\mathbf{k} = \mathbf{k} \times \lambda/k$ can then be introduced and the helical vectors can be defined as

$$\mathbf{h}_{s_k}(\mathbf{k}) = \mathrm{e}^{i s_k \varphi_\mathbf{k}}\ \ (\boldsymbol{\lambda} + i\ s_k\ \boldsymbol{\mu}_\mathbf{k})\ , \tag{10}$$

The angle $\varphi_\mathbf{k}$ defines the rotation around $\mathbf{k}$ needed to transform the basis $(\mu_\mathbf{k}, \lambda)$ onto the basis $(\mathbf{u}_1(\mathbf{k}), \mathbf{u}_2(\mathbf{k}))$. In that sense, since the basis $(\mu_\mathbf{k}, \lambda)$ depends on the triad, the angle $\varphi_\mathbf{k}$ is also a function of $(\mathbf{k}, \mathbf{p}, \mathbf{q})$. The coupling constant for this triad then simply reduces to

$$g(\mathbf{k}, \mathbf{p}, \mathbf{q}, s_k, s_p, s_q) = -\mathrm{e}^{-i(s_k\varphi_\mathbf{k} + s_p\varphi_\mathbf{p} + s_q\varphi_\mathbf{q})}\ s_k\ s_p\ s_q\ \ (s_k \sin\alpha_k + s_p \sin\alpha_p + s_q \sin\alpha_q)\ , \tag{11}$$

$$= -i\ \mathrm{e}^{-i\,\Phi_{kpq}(s_k,s_p,s_q)}\ \ (s_k \sin\alpha_k + s_p \sin\alpha_p + s_q \sin\alpha_q), \tag{12}$$

where the phase $\Phi_{kpq}(s_k, s_p, s_q) = s_k(\varphi_\mathbf{k} + \pi/2) + s_p(\varphi_\mathbf{p} + \pi/2) + s_q(\varphi_\mathbf{q} + \pi/2))$ and α_k, α_p and α_q are defined in Fig. 1 as the interior angles in the triangle formed by the wave vectors $\mathbf{k}$, $\mathbf{p}$ and $\mathbf{q}$ that form a triad ($\mathbf{k} + \mathbf{p} + \mathbf{q} = 0$) and the sines are defined analytically as

$$\sin\alpha_k = \frac{Q}{2\,p\,q} \qquad \sin\alpha_p = \frac{Q}{2\,k\,q} \qquad \sin\alpha_q = \frac{Q}{2\,k\,p}\,, \tag{13}$$

where $Q = \sqrt{2\,k^2\,p^2 + 2\,q^2\,p^2 + 2\,q^2\,k^2 - k^4 - q^4 - p^4}$. The expression (12) shows that g depends only on the shape of the triangle formed by the triad but not on its scale. In the ideal limit ($\nu = \eta = 0$) and in the absence

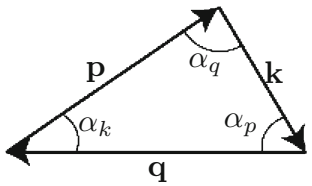

Fig. 1 Representation of the triad formed by the wave vectors **k**, **p** and **q**

of external forcing mechanism, the triadic dynamical system obtained by neglecting all the interactions with wave vectors different from **k**, **p** or **q** reads:

$$\begin{cases} d_t u^{s_k}(\mathbf{k}) = g(\mathbf{k},\mathbf{p},\mathbf{q},s_k,s_p,s_q)\ (s_p p - s_q q)\ (u^{s_p}(\mathbf{p})\,u^{s_q}(\mathbf{q}) - b^{s_p}(\mathbf{p})\,b^{s_q}(\mathbf{q}))^*, \\ d_t u^{s_p}(\mathbf{p}) = g(\mathbf{k},\mathbf{p},\mathbf{q},s_k,s_p,s_q)\ (s_q q - s_k k)\ (u^{s_q}(\mathbf{q})\,u^{s_k}(\mathbf{k}) - b^{s_q}(\mathbf{q})\,b^{s_k}(\mathbf{k}))^*, \\ d_t u^{s_q}(\mathbf{q}) = g(\mathbf{k},\mathbf{p},\mathbf{q},s_k,s_p,s_q)\ (s_k k - s_p p)\ (u^{s_k}(\mathbf{k})\,u^{s_p}(\mathbf{p}) - b^{s_k}(\mathbf{k})\,b^{s_p}(\mathbf{p}))^*, \\ d_t b^{s_k}(\mathbf{k}) = g(\mathbf{k},\mathbf{p},\mathbf{q},s_k,s_p,s_q)\ (-s_k k)\ (u^{s_p}(\mathbf{p})\,b^{s_q}(\mathbf{q}) - b^{s_p}(\mathbf{p})\,u^{s_q}(\mathbf{q}))^*, \\ d_t b^{s_p}(\mathbf{p}) = g(\mathbf{k},\mathbf{p},\mathbf{q},s_k,s_p,s_q)\ (-s_p p)\ (u^{s_q}(\mathbf{q})\,b^{s_k}(\mathbf{k}) - u^{s_q}(\mathbf{q})\,b^{s_k}(\mathbf{k}))^*, \\ d_t b^{s_q}(\mathbf{q}) = g(\mathbf{k},\mathbf{p},\mathbf{q},s_k,s_p,s_q)\ (-s_q q)\ (u^{s_k}(\mathbf{k})\,b^{s_p}(\mathbf{p}) - u^{s_k}(\mathbf{k})\,b^{s_p}(\mathbf{p}))^*. \end{cases} \tag{14}$$

This dynamical system couples six complex variables. The geometric and scale independent g factor is the same in all equations. The second prefactors in (14) only depend on the wave numbers of the triad or, more specifically, on the eigenvalues of the curl operator. The nature of the interaction (14) is obviously affected by the values of the parameters $s_k = \pm 1$, $s_p = \pm 1$ and $s_q = \pm 1$ (eight possible choices). However, the structure of the system is unchanged if all signs s are reversed. Therefore, there are only four different types of interactions.

The expressions for the kinetic helicity H_k and for the ideal MHD invariants are very simple in terms of these helical modes:

$$H_\mathrm{k} = \sum_{\mathbf{k}} k\left(|u^+(\mathbf{k})|^2 - |u^-(\mathbf{k})|^2\right) = \sum_{s_k,\,\mathbf{k}} s_k\, k\, |u^{s_k}(\mathbf{k})|^2 \tag{15}$$

$$E_\mathrm{tot} = \frac{1}{2}\sum_{\mathbf{k}} \left(|u^+(\mathbf{k})|^2 + |u^-(\mathbf{k})|^2 + |b^+(\mathbf{k})|^2 + |b^-(\mathbf{k})|^2\right) \tag{16}$$

$$H_\mathrm{c} = \sum_{\mathbf{k}} \Re\left(u^+(\mathbf{k})b^+(\mathbf{k})^* + u^-(\mathbf{k})b^-(\mathbf{k})^*\right) \tag{17}$$

$$H_\mathrm{m} = \sum_{\mathbf{k}} \frac{1}{k}\left(|b^+(\mathbf{k})|^2 - |b^-(\mathbf{k})|^2\right), \tag{18}$$

where E_tot is the total energy, H_c the cross-helicity and H_m the magnetic helicity. The symbol $\Re$ represents the real part of a complex number. The dynamical system (14) automatically conserves these invariants, independently of the values of **k**, **p** and **q**.

3 Shell models for MHD turbulence

Shell models have been first introduced for studying high Reynolds number fluid turbulence. In particular, the so-called GOY [2,4] and SABRA [5,6] models have been quite successful in describing the energy fluxes and spectra for fluid turbulence. Shell models also have been developed for MHD turbulence, see [7] for the pioneering work and [8–10] for more recent extensions of the GOY model to MHD turbulence.

In those models, the Fourier space is split into spheres centred at the origin with radii in a geometric progression of ratio λ. All wave vectors lying between two successive spheres (i.e. within a shell) are traditionally represented by one complex scalar number. This complex variable accounts for the state of the field in the range of scales corresponding to the wave numbers of the shell. This construction tremendously diminishes the number of variables in the system, thereby allowing for simulations of very high Reynolds numbers. The

price to pay is that all the geometrical features of turbulence are lost in the process. In general, this loss is not considered as a real issue since the main purpose of the shell models is to explore the dynamics of the energy cascade for homogeneous turbulence in a range of scale that are considered as unaffected by the actual boundary conditions of the flow. Nevertheless, even in such conditions, some quantities are not easily represented by complex scalar numbers. For instance, the helicity represents the alignment between the velocity and the vorticity vectors. In general, the characteristic helicity associated with an ensemble of wave vectors cannot be inferred from the knowledge of their average energy. However, in many shell models used both for fluid and MHD turbulence [2,4–6,8,9], the helicity and the energy in a shell are not treated as independent quantities. In these models, the helicity within a shell is simply given by the energy within this shell multiplied by $\pm k$, with the sign "+" and "−" changing alternatively between successive shells. This situation has long been recognised as poorly satisfactory and, inspired by the helical decomposition of NS equations [13], Benzi et al. [12] proposed an extension of the GOY shell model with two scalar variables per shell. For each scale, there is now one variable accounting for each helical projection and the energy and the helicity in a shell are no longer linked.

This helical model for fluid turbulence has equations of evolution that mimic the Navier–Stokes equations. The interactions are triadic and local interactions are assumed to limit the couplings to first and second neighbouring shells. The structure of the non-linear terms is then fixed and the coefficient are determined to ensure that the nonlinear terms conserve the two Navier–Stokes invariants. However, all the coefficients cannot be prescribed and four parameters remain undetermined leading to four classes of a *priori* independent models.

3.1 Shell models based on triadic dynamical systems

In the following, shell models are derived using a somewhat different technique (see also [14]). Extending the approach of [12] to MHD, two complex variables are used to characterise each of the MHD fields in the shell n (velocity or magnetic): U_n^+, U_n^-, B_n^+, and B_n^-. However, instead of considering the general coupling between neighbouring shells, three shells with labels n, $n+\ell_1$ and $n+\ell_2$ are coupled by simply transposing the dynamical system (14) into dynamical evolution equations for the shell variables:

$$\left\{\begin{array}{rl}
d_t U_n^{s_n} &= \mathcal{G}_{n,n+\ell_1,n+\ell_2}^{s_n,s_{n+\ell_1},s_{n+\ell_1}}\ k_0\lambda^n\ (s_{n+\ell_1}\lambda^{\ell_1} - s_{n+\ell_2}\lambda^{\ell_2})\ (U_{n+\ell_1}^{s_{n+\ell_1}}\, U_{n+\ell_2}^{s_{n+\ell_2}} - B_{n+\ell_1}^{s_{n+\ell_1}}\, B_{n+2}^{s_{n+2}})^*,\\
d_t U_{n+\ell_1}^{s_{n+\ell_1}} &= \mathcal{G}_{n,n+\ell_1,n+\ell_2}^{s_n,s_{n+\ell_1},s_{n+\ell_1}}\ k_0\lambda^n\ (s_{n+\ell_2}\lambda^{\ell_2} - s_n)\ (U_{n+\ell_2}^{s_{n+\ell_2}}\, U_n^{s_n} - B_{n+\ell_2}^{s_{n+\ell_2}}\, B_n^{s_n})^*,\\
d_t U_{n+\ell_2}^{s_{n+\ell_2}} &= \mathcal{G}_{n,n+\ell_1,n+\ell_2}^{s_n,s_{n+\ell_1},s_{n+\ell_1}}\ k_0\lambda^n\ (s_n - s_{n+\ell_1}\lambda^{\ell_1})\ (U_n^{s_n}\, U_{n+\ell_1}^{s_{n+\ell_1}} - B_n^{s_n}\, B_{n+\ell_1}^{s_{n+\ell_1}})^*,\\
d_t B_n^{s_n} &= \mathcal{G}_{n,n+\ell_1,n+\ell_2}^{s_n,s_{n+\ell_1},s_{n+\ell_1}}\ k_0\lambda^n\ (-s_n)\ (U_{n+\ell_1}^{s_{n+\ell_1}}\, B_{n+\ell_2}^{s_{n+\ell_2}} - B_{n+\ell_1}^{s_{n+\ell_1}}\, U_{n+\ell_2}^{s_{n+\ell_2}})^*,\\
d_t B_{n+\ell_1}^{s_{n+\ell_1}} &= \mathcal{G}_{n,n+\ell_1,n+\ell_2}^{s_n,s_{n+\ell_1},s_{n+\ell_1}}\ k_0\lambda^n\ (-s_{n+\ell_1}\lambda^{\ell_1})\ (U_{n+\ell_2}^{s_{n+\ell_2}}\, B_n^{s_n} - B_{n+\ell_2}^{s_{n+\ell_2}}\, U_n^{s_n})^*,\\
d_t B_{n+\ell_2}^{s_{n+\ell_2}} &= \mathcal{G}_{n,n+\ell_1,n+\ell_2}^{s_n,s_{n+\ell_1},s_{n+\ell_1}}\ k_0\lambda^n\ (-s_{n+\ell_2}\lambda^{\ell_2})\ (U_n^{s_n}\, B_{n+\ell_1}^{s_{n+\ell_1}} - B_n^{s_n}\, U_{n+\ell_1}^{s_{n+\ell_1}})^*,
\end{array}\right. \tag{19}$$

where the integers ℓ_1 and ℓ_2 can be either positive or negative, and $\mathcal{G}$ is a coupling constant that remains to be determined. Indeed, in the dynamical system (14), the constant g is fully determined by the structure of the MHD equations. In the construction of the shell model, $\mathcal{G}$ can be interpreted as an "averaged" coupling constant between all the interacting triads coupling three shells. It cannot, however, be derived without additional assumption. Since the original coupling constant $g(\mathbf{k}, \mathbf{p}, \mathbf{q}, s_k, s_p, s_q)$ is scale independent, it is reasonable to assume that the effective coupling constant $\mathcal{G}$ has the same property. In the following, the notation,

$$\mathcal{G}_{n,n+\ell_1,n+\ell_2}^{s_n,s_{n+\ell_1},s_{n+\ell_2}} = G_{\ell_1,\ell_2}^{s_n,s_{n+\ell_1},s_{n+\ell_2}}\,, \tag{20}$$

will be used systematically to emphasise this scale invariance. A large number of couplings can be considered but some of them are forbidden [15]. For instance two shells with small characteristic wave numbers cannot interact with a third shell with a very large characteristic wave number because of the triad constraint. Keeping only some of these interactions cannot be justified except by using some phenomenology arguments. Considering the expression of the original coupling constant $g(\mathbf{k}, \mathbf{p}, \mathbf{q}, s_k, s_p, s_q)$, it is, however, reasonable to assume that the effective coupling constant can be described by a typical triad characteristic of the shells $(n, n+\ell_1, n+\ell_2)$, an amplitude that depends only on the distance between the shells and a phase:

$$G_{\ell_1,\ell_2}^{s_n,s_{n+\ell_1},s_{n+\ell_2}} = -i\ \mathrm{e}^{-i\overline{\Phi}_{\ell_1,\ell_2}(s_n,s_{n+\ell_1},s_{n+\ell_2})}\ A_{\ell_1,\ell_2}\ \left(s_n\ \sin\overline{\alpha}_k^{\ell_1,\ell_2} + s_{n+\ell_1}\ \sin\overline{\alpha}_p^{\ell_1,\ell_2} + s_{n+\ell_2}\ \sin\overline{\alpha}_q^{\ell_1,\ell_2}\right). \tag{21}$$

The angles of the triad $\overline{\alpha}_k^{\ell_1,\ell_2}, \overline{\alpha}_p^{\ell_1,\ell_2}$ and $\overline{\alpha}_q^{\ell_1,\ell_2}$ depend on the distance between the shells but not on the eigenvalues of the curl operator. The scaling A_{ℓ_1,ℓ_2} results from at least two properties with opposite effects. First, it is tempting to assume that A_{ℓ_1,ℓ_2} is a growing function of ℓ_1 and ℓ_2. Indeed, for a given n, there is an increasing number of possible triads when interactions with shells $n+\ell_1$ and $n+\ell_2$ are considered. However, the actual velocity and magnetic field modes in distant shells might be less correlated with modes in shell n, yielding to a huge number of seemingly random interactions that could very much cancel each other. Assuming that predominance of local interactions would suggest to introduce a decreasing amplitude factor A_{ℓ_1,ℓ_2} for increasing ℓ_1 and ℓ_2 as in [15]. Typically, assuming that the energy cascades are dominated by local interactions, it is very common to keep only local interactions between three different shells in the model (all the $A_{\ell_1,\ell_2} = 0$, except $A_{1,2}$). In this case, only the choice $(\ell_1, \ell_2) = (-2,-1), (-1,+1), (+1,+2)$ is taken into account. Moreover, taking into account the scale invariance of the coupling constants, the following relations can be derived:

$$\begin{aligned}\mathcal{G}_{n,n-1,n+1}^{s_n,s_{n-1},s_{n+1}} &= \mathcal{G}_{n-1,n,n+1}^{s_{n-1},s_n,s_{n+1}} = \mathcal{G}_{n,n+1,n+2}^{s_{n-1},s_n,s_{n+1}},\\ \mathcal{G}_{n,n-2,n-1}^{s_n,s_{n-2},s_{n-1}} &= \mathcal{G}_{n-2,n-1,n}^{s_{n-2},s_{n-1},s_n} = \mathcal{G}_{n,n+1,n+2}^{s_{n-2},s_{n-1},s_n}.\end{aligned}$$

Taking into account these relation, the general model with interactions between three different successive shells only reads:

$$\begin{aligned}(d_t+\nu k_n^2)\,U_n^{s_n} - f_n = k_n \Bigg(&\sum_{s_{n+1},s_{n+2}} G_{1,2}^{s_n,s_{n+1},s_{n+2}} (s_{n+1}\lambda - s_{n+2}\lambda^2)(U_{n+1}^{s_{n+1}}\,U_{n+2}^{s_{n+2}} - B_{n+1}^{s_{n+1}}\,B_{n+2}^{s_{n+2}})^*\\ &+ \sum_{s_{n-1},s_{n+1}} G_{1,2}^{s_{n-1},s_n,s_{n+1}} (s_{n-1}\lambda^{-1} - s_{n+1}\lambda)(U_{n+1}^{s_{n+1}}\,U_{n-1}^{s_{n-1}} - B_{n+1}^{s_{n+1}}\,B_{n-1}^{s_{n-1}})^*\\ &+ \sum_{s_{n-1},s_{n-2}} G_{1,2}^{s_{n-2},s_{n-1},s_n} (s_{n-2}\lambda^{-2} - s_{n-1}\lambda^{-1})(U_{n-2}^{s_{n-2}}\,U_{n-1}^{s_{n-1}} - B_{n-2}^{s_{n-2}}\,B_{n-1}^{s_{n-1}})^* \Bigg),\\ (d_t+\eta k_n^2)\,B_n^{s_n} = -s_n k_n \Bigg(&\sum_{s_{n+1},s_{n+2}=\pm} G_{1,2}^{s_n,s_{n+1},s_{n+2}} (U_{n+1}^{s_{n+1}}\,B_{n+2}^{s_{n+2}} - B_{n+1}^{s_{n+1}}\,U_{n+2}^{s_{n+2}})^*\\ &+ \sum_{s_{n-1},s_{n+1}=\pm} G_{1,2}^{s_{n-1},s_n,s_{n+1}} (U_{n+1}^{s_{n+1}}\,B_{n-1}^{s_{n-1}} - B_{n+1}^{s_{n+1}}\,U_{n-1}^{s_{n-1}})^*\\ &+ \sum_{s_{n-1},s_{n-2}=\pm} G_{1,2}^{s_{n-2},s_{n-1},s_n} (U_{n-2}^{s_{n-2}}\,B_{n-1}^{s_{n-1}} - B_{n-2}^{s_{n-2}}\,U_{n-1}^{s_{n-1}})^* \Bigg).\end{aligned} \tag{22}$$

By construction, this shell model automatically conserves the MHD ideal invariants that are expressed in terms of the shell variables as:

$$E_{\mathrm{tot}} = \frac{1}{2}\sum_n \left(|U_n^+|^2 + |U_n^-|^2 + |B_n^+|^2 + |B_n^-|^2\right) \tag{23}$$

$$H_{\mathrm{c}} = \sum_n \Re\left(U_n^+ B_n^{+\,*} + U_n^- B_n^{-\,*}\right) \tag{24}$$

$$H_{\mathrm{m}} = \sum_n \frac{1}{k_n}\left(|B_n^+|^2 - |B_n^-|^2\right) \tag{25}$$

and, in the limit of vanishing magnetic field ($B_n = 0$), the kinetic helicity

$$H_{\mathrm{k}} = \sum_n k_n \left(|U_n^+|^2 - |U_n^-|^2\right) \tag{26}$$

is also automatically conserved. However, the coupling constants G are still unknown at this stage and, like in the same approach applied to Navier–Stokes turbulence, four independent effective coupling constants $G_{1,2}^{+,+,+}$, $G_{1,2}^{+,+,-}$, $G_{1,2}^{+,-,+}$ and $G_{1,2}^{-,+,+}$ have to be determined. The other four effective coupling constants are obtained using the property $G_{1,2}^{-s_k,-s_p,-s_q} = G_{1,2}^{s_k,s_p,s_q\,*}$.

3.2 Evaluation of the coupling constants

In order to complete the definition of the shell model, the coupling constants have to be determined. Indeed, even if the shell model contains only local interactions characterised by $\ell_1 = 1$ and $\ell_2 = 2$, four effective G remain unknown. In practice, both the phase $\overline{\Phi}_{1,2}(s_n, s_{n+1}, s_{n+2})$ and the angles $\overline{\alpha_k}^{1,2}$ have to be determined.

In order to determine the angles $\overline{\alpha}^{1,2}$, an averaging procedure over all triplets of wave vectors such that $\mathbf{k} \in S_n$, $\mathbf{p} \in S_{n+1}$ and $\mathbf{q} \in S_{n+2}$ that form triads can easily be defined. Here, S_n represents the shell n. First, the integral over all these wave vectors is introduced:

$$I[A(\mathbf{k},\mathbf{p},\mathbf{q})]_{n,n+1,n+2} \equiv \int_{\mathbf{k}\in S_n} \mathrm{d}\mathbf{k} \int_{\mathbf{p}\in S_{n+1}} \mathrm{d}\mathbf{p} \int_{\mathbf{q}\in S_{n+2}} \mathrm{d}\mathbf{q}\, A(\mathbf{k},\mathbf{p},\mathbf{q})\, \delta(\mathbf{k}+\mathbf{p}+\mathbf{q}), \tag{27}$$

where $A(\mathbf{k},\mathbf{p},\mathbf{q})$ is an arbitrary function of the wave vectors $(\mathbf{k},\mathbf{p},\mathbf{q})$. If this function is scale independent, the "triad-average" is simply defined by

$$\langle A(\mathbf{k},\mathbf{p},\mathbf{q})\rangle_{\{1,2\}} = I[A(\mathbf{k},\mathbf{p},\mathbf{q})]_{n,n+1,n+2} \,/\, I[1]_{n,n+1,n+2}\,, \tag{28}$$

where the subscripts $\{1, 2\}$ refer again to $\ell_1 = 1$ and $\ell_2 = 2$. Of course, the result of this averaging depends on the value chosen for λ. In the original works on shell models, the choice $\lambda = 2$ was systematically adopted, although some sensitivity studies have been proposed. For instance, $\lambda = 1.5$, $\lambda = 2.5$ and even the limit $\lambda \to 1$ have been explored in [12]. The value $\lambda = (1+\sqrt{5})/2$ has been introduced by several authors [5,9,16]. This particular choice of λ ensures that, for any value of q in the shell $n+2$, it is possible to find values of k and p, respectively, in shells n and $n+1$ that correspond to a triad. Another interesting choice would be the limit λ_* for which any choice of k, p and q in shells n, $n+1$ and $n+2$ would be acceptable for a triad. The value of $\lambda_* \approx 1.3247$ satisfies $\lambda_*^3 - \lambda_* - 1 = 0$. For any $\lambda \le \lambda_*$, all the choices of (k, p, q) in successive shell do interact through at least one triad. The other advantage is that when $\lambda \le \lambda_*$, the triad-average values of k, p, q, defined using (28) satisfy $\langle p\rangle_{\{1,2\}}/\langle k\rangle_{\{1,2\}} = \langle q\rangle_{\{1,2\}}/\langle p\rangle_{\{1,2\}} = \lambda$. These values thus grow exactly like the shell widths.

Although this choice is interesting, the golden number $\lambda = (1+\sqrt{5})/2$ has been adopted in the following since it corresponds to the value chosen in the most recent shell model studies of MHD turbulence [9,15]. The average values of k, p and q are then given by

$$\begin{cases} \overline{k} = \langle k\rangle_{\{1,2\}} = \left(\dfrac{9624}{12245} + \dfrac{3216}{12245}\sqrt{5}\right) k_0\,\lambda^n \approx 1.373\, k_0\,\lambda^n \\ \overline{p} = \langle p\rangle_{\{1,2\}} = \left(\dfrac{13458}{12245} + \dfrac{6366}{12245}\sqrt{5}\right) k_0\,\lambda^n \approx 2.262\, k_0\,\lambda^n \\ \overline{q} = \langle q\rangle_{\{1,2\}} = \left(\dfrac{19818}{12245} + \dfrac{8418}{12245}\sqrt{5}\right) k_0\,\lambda^n \approx 3.156\, k_0\,\lambda^n \end{cases}. \tag{29}$$

These values allow to propose an effective triad for which the angles $(\overline{\alpha}_k, \overline{\alpha}_p, \overline{\alpha}_q)$ are defined using the formula (13) but with the effective values of the wave numbers (29). The following values are obtained: $\sin\overline{\alpha}_k^{1,2} = 0.383$, $\sin\overline{\alpha}_p^{1,2} = 0.630$ and $\sin\overline{\alpha}_q^{1,2} = 0.879$.

We now focus on the effective phase $\overline{\Phi}_{1,2}(s_n, s_{n+1}, s_{n+2})$. As the original phase in (12), it is expected to be linear in the helicity signs: $\overline{\Phi}_{1,2} = s_n\overline{\phi}_k + s_{n+1}\overline{\phi}_p + s_{n+2}\overline{\phi}_q$, where the effective angles $\overline{\phi}_k$, $\overline{\phi}_p$, and $\overline{\phi}_q$ have to be determined. Various choices have been explored. In particular, if the effective phase is a symmetric function of the three helicity signs, the model is reminiscent of two-dimensional turbulence. Indeed, in that case, the three effective angles $(\overline{\phi}_k, \overline{\phi}_p, \overline{\phi}_q)$ are identical and are equal to $\overline{\phi}$ and $\overline{\Phi}_{1,2} = (s_n + s_{n+1} + s_{n+2})\overline{\phi}$. It is then possible to define the following quantity $a_n = u_n^+ \mathrm{e}^{i\overline{\phi}} + u_n^- \mathrm{e}^{-i\overline{\phi}}$ for which the evolution equation in the absence of magnetic field is readily derived, assuming $\lambda \le \lambda^*$:

$$(d_t + \nu k_n^2)a_n = -2\,i\,k_n\,\sin\alpha_k\,\left((\lambda^2-\lambda^4)\,a_{n+1}^* a_{n+2}^* + \lambda(\lambda^2-\lambda^{-2})\,a_{n-1}^* a_{n+1}^* + \lambda^2(\lambda^{-4}-\lambda^{-2})a_{n-2}^* a_{n-1}^*\right).$$

The choice $\lambda \le \lambda^*$ is important to simplify the evolution equation since it implies $\langle p\rangle_{\{1,2\}}/\langle k\rangle_{\{1,2\}} = \langle q\rangle_{\{1,2\}}/\langle p\rangle_{\{1,2\}} = \lambda$. In that case, it is easy to show that both $\sum_n |a_n|^2$ and $\sum_n k_n^2|a_n|^2$ are conserved by the nonlinear terms. There are thus two positively defined quadratic invariants that can be identified as the

energy and the enstrophy. The equations for the a_ns therefore correspond to a shell model for 2D turbulence when $\lambda \leq \lambda^*$. For this reason and despite the fact that in the simulation the value of λ is larger than λ^*, the choice of phases that has been retained in the model deliberately avoids $\overline{\phi}_k = \overline{\phi}_p = \overline{\phi}_q$:

$$\overline{\Phi}_{1,2}(s_n, s_{n+1}, s_{n+2}) = s_n\,\pi + (s_{n+1} + s_{n+2})\frac{\pi}{2} \tag{30}$$

which gives after some simple algebraic manipulations:

$$G_{1,2}^{s_n,s_{n+1},s_{n+2}} = -i\ A_{1,2}\ s_{n+1}\ s_{n+2}\ \left(s_n\ \sin\overline{\alpha}_k^{1,2} + s_{n+1}\ \sin\overline{\alpha}_p^{1,2} + s_{n+2}\ \sin\overline{\alpha}_q^{1,2}\right). \tag{31}$$

The choice (30) is arbitrary (see also [15]). It only ensures to avoid the two-dimensionalisation. Finally, the value $A_{1,2} = 1$ has been chosen without loss of generality since this parameter can be lumped into the definition of a new time scale. The effective coupling constants are then given by (31) completed by $A_{1,2} = 1$ and by the values of the sines given after formula (29).

This expression completes the definition of the helical shell model for MHD (and NS as well) since it explicitly determines all four effective coupling constants needed in the shell model.

4 Results

4.1 Numerical experiments

The shell model equations (22) in which the shell aspect ratio is given by $\lambda = (1+\sqrt{5})/2$ and the effective coupling constants are given by (31) have been numerically evolved using a fourth-order Runge–Kutta method with an adaptive time-step procedure. In each run, the system was evolved for 10^8 time steps. Each point in the time series represented below is obtained by average over 5×10^5 successive time steps. In this averaging, the data are however recorded every five time steps to increase the computational performances. The following forcing has been applied:

$$f_{n_\mathrm{f}}^+ = \epsilon^+ \frac{\mathrm{e}^{i\phi_1}}{\cos(\phi_1)} \frac{u_{n_\mathrm{f}}^+}{|u_{n_\mathrm{f}}^+|^2}, \qquad f_{n_\mathrm{f}}^- = \epsilon^- \frac{\mathrm{e}^{i\phi_2}}{\cos(\phi_2)} \frac{u_{n_\mathrm{f}}^-}{|u_{n_\mathrm{f}}^-|^2}, \tag{32}$$

where ϵ^+ and ϵ^- are real numbers; n_f is the index of the forced shell and is taken to be $n_\mathrm{f} = 4$ so that a full triad of "large" scale exists. The forcing is acting only on this shell ($f_n^\pm = 0 \ \ \forall n \neq n_\mathrm{f},$). The rate of energy injection is therefore $\epsilon = \epsilon^+ + \epsilon^-$. The forcing amplitudes ϵ^+ and ϵ^- are both assumed to be positive numbers. Indeed, if one of these amplitudes is negative, energy would be extracted from the corresponding forced modes at a constant rate. This would unavoidably lead to $u_{n_\mathrm{f}}^+ = 0$ or $u_{n_\mathrm{f}}^- = 0$ and, considering the structure of the forcing, to instabilities. The kinetic helicity injection rate is $(\epsilon^+ - \epsilon^-)\ k_{n_\mathrm{f}}$. The phases ϕ_1 and ϕ_2 are introduced to avoid the "dynamical alignment" described in [17] and to ensure that the injected cross-helicity rate vanishes. In general, it is expected that a helical forcing eases the apparition of the magnetic field. The Riga [18,19] and Karlsruhe [20] experiments are, for instance, designed in such a way that the fluid motion is helical. In the shell models based on helical modes, the forcing can inject helicity ($\epsilon^+ \neq \epsilon^-$) or not ($\epsilon^+ = \epsilon^-$). In the following, a first simulation shows that our model correctly compares with earlier results concerning Navier–Stokes turbulence. Finally, the influence of the helicity of the forcing on the steady states reached by the MHD model is studied.

4.2 Navier–Stokes turbulence

Setting the magnetic field $B = 0$ to zero in (22) leads to a model of NS turbulence. It is thus possible to validate our model in comparison with the results obtained by the GOY and Benzi et al. models. The results of this section were obtained by evolving our model with $N = 36$ shells, viscosity $\nu = 10^{-7}$, $\lambda = (1+\sqrt{5})/2$ and $k_1 = 2^{-3}$ and the forcing $f_4^\pm = 5\ (1+i)\ 10^{-3}$. The GOY model and the third model of Benzi et al. [12] have been evolved in the conditions of this latter reference ($N = 22$, $\nu = 10^{-7}$, $\lambda = 2$ and $k_1 = 2^{-3}$).

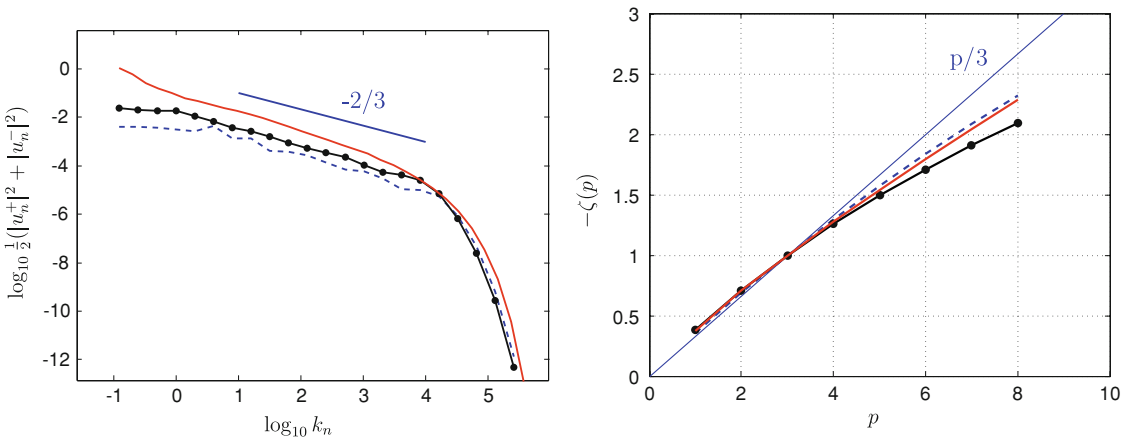

Fig. 2 Energy spectra (*left*) together with scaling exponents (*right*). GOY model: *blue/dashed*. Third model of Benzi et al. [12]: *black/dotted line*. Our model: *red/line*. Kolmogorov's $\zeta(p) = -p/3$ law: straight blue line (right panel) (Color figure online)

The energy spectra are presented in the left panel of Fig.2. There is general agreement as long as the $-5/3$ law is concerned (translated into a $-2/3$ law in shell models as the energy in each shell is displayed rather than the spectral density of energy).

The scaling exponents $\zeta(p)$ defined by $S_p(n) = \langle |u_n|^p \rangle \sim k_n^{-\zeta(p)}$ and calculated using extended self-similarity [21] are displayed in Fig.2, right panel, for the three models together with Kolmogorov's $\zeta(p) = -p/3$ prediction.

4.3 Influence of helicity injection on the onset of dynamo

This section focuses on MHD simulations with Reynolds number close to criticality for the onset of dynamo. The number of shells is $N = 25$, $\nu = 10^{-7}$, $\eta = 10^{-4}$ and $k_1 = 1.17$. Two series of runs have been performed with the forcing (32). One of them corresponds to no helicity injection ($\epsilon^+ = \epsilon^- = \epsilon/2$) and the other one to maximal helicity injection ($\epsilon^+ = \epsilon, \epsilon^- = 0$). They will be referred to as the non-helical and the helical runs, respectively.

In both cases, a first simulation with $\epsilon = \epsilon_0 \equiv 10^{-10}$ is performed until a statistically stationary regime is reached. The run is then stopped and restarted with a new value of the energy injection rate $\epsilon_1 = (3/2)^3\,\epsilon_0$. This choice corresponds to an increase of the Reynolds number $R_e = (k_\nu/k_f)^{4/3}$ by a factor 3/2 since the viscous wave vector is given by

$$k_\nu = \left(\frac{\epsilon}{\nu^3}\right)^{1/4}. \tag{33}$$

The same procedure is then reproduced with $\epsilon_2 = (3/2)^3\,\epsilon_1$ and $\epsilon_3 = (3/2)^3\,\epsilon_2$.

When the magnetic field has decayed too much (especially with ϵ_0 and ϵ_1), a small seed magnetic field is used to re-initialise the magnetic field shell variables before restarting the simulation. The evolution of the kinetic and magnetic energies is shown in Fig. 3. Several differences are observed. First, the energy evolution seems to be more intermittent in the non-helical runs. Second, a sustained magnetic field is observed for a smaller value of the energy injection rate in the helical runs. This indicates that the dynamo effect may be more easily observed with an helical forcing. Since the parameters in these runs correspond to Reynolds numbers just above the critical limit for ϵ_2 (helical run only) and ϵ_3 (both helical and non-helical runs), the magnetic energy remains fairly low. It has been checked however that it does not tend to vanish for longer time by performing very long runs. Although the magnetic energy is small, the magnetic field is responsible for a significant fraction of the dissipation since $\eta = 10^3\nu$. This explains why the kinetic energy levels are significantly lower in the helical runs once the dynamo regime is reached. Indeed, a fraction of the energy injection is transferred to the magnetic field to compensate for the Joule dissipation.

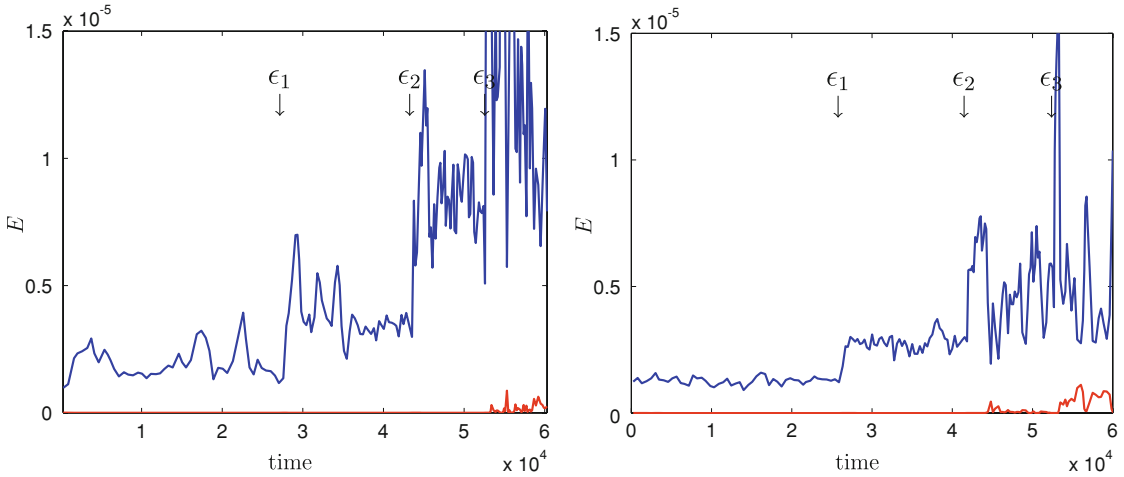

Fig. 3 Kinetic (*blue/upper*) and magnetic (*red/lower*) energies versus time. The simulations are started with $\epsilon = \epsilon_0 \equiv 10^{-10}$ and, at the times indicated by the *arrows*, the energy injection rate is successively increased to ϵ_1, ϵ_2 and ϵ_3. The time for all runs are non-dimensionalised using $\tau_\nu = (\nu\, k_\nu^2)^{-1}$ in which k_ν (33) has been computed with ϵ_0. The *left figure* corresponds to non-helical runs and the *right figure* to the helical runs (Color figure online)

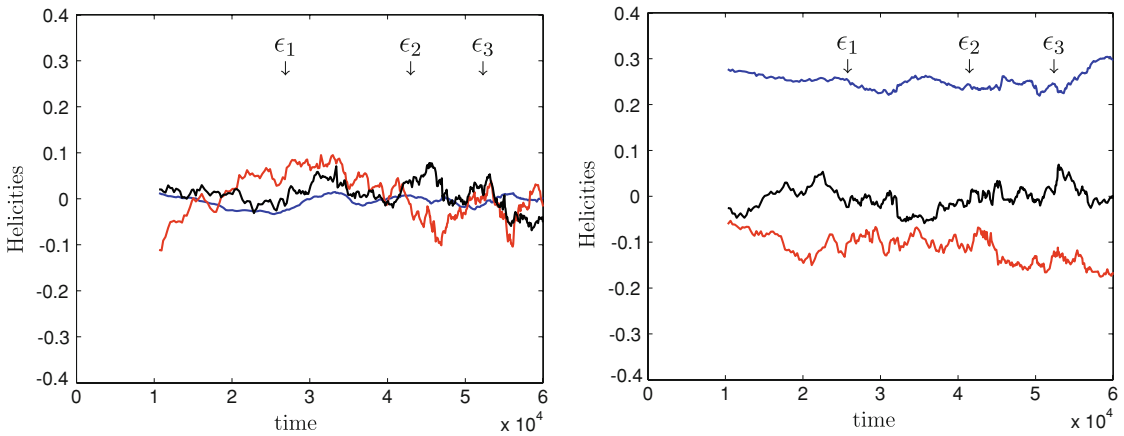

Fig. 4 Kinetic $\overline{H}_\mathrm{k}$ (*blue/grey* less oscillating), magnetic $\overline{H}_\mathrm{m}$ (*red/grey* more oscillating) and cross $\overline{H}_\mathrm{c}$ (*black*) helicities versus time. The parameters of the runs are the same as for Fig. 3 (Color figure online)

The kinetic, magnetic and cross helicities are reported in Fig. 4 in the following non-dimensional form:

$$\overline{H}_\mathrm{k} = \left(\sum_n k_n \left(|U_n^+|^2 - |U_n^-|^2\right)\right) \Big/ \left(\sum_n k_n \left(|U_n^+|^2 + |U_n^-|^2\right)\right) \tag{34}$$

$$\overline{H}_\mathrm{m} = \left(\sum_n \frac{1}{k_n} \left(|B_n^+|^2 - |B_n^-|^2\right)\right) \Big/ \left(\sum_n \frac{1}{k_n} \left(|B_n^+|^2 + |B_n^-|^2\right)\right) \tag{35}$$

$$\overline{H}_\mathrm{c} = \left(\sum_n \Re\left(U_n^+ B_n^{+\,*} + U_n^- B_n^{-\,*}\right)\right) \Big/ \sqrt{E_\mathrm{k}\, E_\mathrm{m}}, \tag{36}$$

where E_k and E_m are the kinetic and magnetic energies. Because the helicities appear to be highly fluctuating quantities, the values reported in Fig. 4 correspond to local time averaging based on the recent past history. This explains why these graphs do not start at $t = 0$. The advantage of using the non-dimensional form of the helicities is that the results are almost independent of the energy injection rate. Quite remarkably, even in the decaying magnetic field regimes, before the onset of the dynamo, the non-dimensional cross and magnetic helicities are very stable on average. In the non-helical runs, all helicities appear to fluctuate around zero. As

expected, a non-zero kinetic helicity is observed in the helical runs. Interestingly, a magnetic helicity also develops, but with an opposite sign.

5 Conclusions

The helical decomposition of the Navier–Stokes equations [13] has been extended to MHD. Moreover, the helical shell models introduced by Benzi et al. [12] have also been adapted to MHD. However, the usual approach to derive shell models (imposing the conservation of quadratic invariants) leads to as many models as different types of triad involved. We have therefore proposed a different approach for the construction of shell models by copying the system of dynamical equations typical of a triad in MHD directly in the formalism of the shell variables. This simple procedure both gives the model's coefficients at once (avoiding lengthy algebra in the writing of the conservation laws especially for MHD) and leads to a natural definition of the weights (the effective coupling constants) to be applied to the different triads. This allows in particular to build a shell model presenting all four types of helical interactions.

The investigation of this model has shown that it is very simple to design numerical experiments in which a fixed injection rate of kinetic helicity is imposed. These models are thus perfectly adapted to the analysis of the effect of helicity injection on MHD turbulence and, more specifically on the observation of a dynamo effect. Also, the formalism proposed here is very well suited to the exploration of other coupling terms between the shells.

The numerical results obtained in Sect. 4.2 indicates that the dynamo effect may be more easily observed with an helical forcing. Indeed, in the series of run with helical forcing, a sustained magnetic field is observed for a lower energy injection rate than in the series of run with a non-helical forcing. The observation of an influence of the helicity injection rate on the onset of dynamo is quite remarkable since shell model have been designed for exploring the behaviour of high Reynolds number turbulence. Indeed, although the velocity shell variables do correspond to a fully developed turbulent regime, clearly, close to the onset of dynamo, the magnetic shell variables cannot be considered as fully turbulent. It must be acknowledged that, despite the encouraging observation presented here, the relevance of shell models close to a transition is not fully established and may require more investigation.

It must be acknowledged also that, although a fairly robust procedure has been proposed to estimate the effective coupling constant in the shell models, a sensitivity study of the choice of the shell width λ on the results should probably be considered for these helical models. Moreover, the choice (30) for the effective phase $\overline{\Phi}$ that appears in the coupling constants has not been justified so far.

Acknowledgements This work has been partly supported by the contract of association EURATOM—Belgian state. D.C. and T.L. are supported by the Fonds de la Recherche Scientifique (Belgium).

References

1. Frisch, U.: Turbulence: The Legacy of A.N. Kolmogorov. Cambridge University Press, Cambridge (1995)
2. Gletzer, E.B.: System of hydrodynamic type admitting two quadratic integrals of motion. Sov. Phys. Dokl. **18**, 216–217 (1973)
3. Lorenz, E.N.: Low order models representing realizations of turbulence. J. Fluid Mech. **55**, 545–563 (1972)
4. Yamada, M., Ohkitani, K.: Lyapounov spectrum of a chaotic model of three-dimensional turbulence. J. Phys. Soc. Jpn. **56**, 4210–4213 (1987)
5. L'vov, V.S., Podivilov, E., Pomyalov, A., Procaccia, I., Vandembroucq, D.: Improved shell model of turbulence. Phys. Rev. E **58**, 1811–1822 (1998)
6. L'vov, V.S., Podivilov, E., Procaccia, I.: Hamiltonian structure of the Sabra shell model of turbulence: exact calculation of an anomalous scaling exponent. Europhys. Lett. **46**, 609–612 (1999)
7. Gloaguen, C., Léorat, J., Pouquet, A., Grappin, R.: A scalar model for MHD turbulence. Physica D **17**, 154–182 (1985)
8. Frick, P., Sokoloff, S.: Cascade and dynamo action in a shell model of magnetohydrodynamic turbulence. Phys. Rev. E **57**, 4155–4164 (1998)
9. Stepanov, R., Plunian, F.: Fully developed turbulent dynamo at low magnetic prandtl numbers. J. Turbul. **7**(39), (2006)
10. Lessinnes, T., Verma, M., Carati, D.: Energy transfers in shell models of magnetohydrodynamic turbulence. Phys. Rev. E arxiv:0807.5076 (2008)
11. Stepanov, R., Plunian, F.: Phenomenology of turbulent dynamo growth and saturation. Astrophys. J. **680**, 809–815 (2008)
12. Benzi, R., Biferale, L., Kerr, R.M., Trovatore, E.: Helical shell models for three-dimensional turbulence. Phys. Rev. E **53**, 3541–3550 (1996)
13. Waleffe, F.: The nature of triad interactions in homogeneous turbulence. Phys. Fluids A **4**, 350–363 (1992)

14. Lessinnes, T., Carati, D.: Helical shell models for MHD turbulence. In: Proceeding of the 7th Int. PAMIR Conf. vol. 2, pp. 513–524 (2008); Lessinnes, T., Carati, D.: Helical shell models for MHD turbulence. Magnetohydrodynamics **45**(2), 193–202 (2009)
15. Plunian, F., Stepanov, R.: A non-local shell model of hydrodynamic and magnetohydrodynamic turbulence. New J. Phys. **9**, 294–319 (2007)
16. Ottinger, J.L., Carati, D.: Shell models for plasma turbulence. Phys. Rev. E **48**, 2955–2965 (1993)
17. Giuliani, P., Carbone, V.: A note on shell models for mhd turbulence. Europhys. Lett. **43**(5), 527–532 (1998)
18. Gailitis, A., Lielausis, O., Platacis, E., Dement'ev, S., Cifersons, A., Gerbeth, G., Gundrum, T., Stefani, F., Christen, M., Hänel, H., Will, G.: Detection of a flow induced magnetic field eigenmode in the riga dynamo facility. Phys. Rev. Lett. **84**, 4365–4368 (2000)
19. Gailitis, A., Lielausis, O., Dement'ev, S., Platacis, E., Cifersons, A., Gerbeth, G., Gundrum, T., Stefani, F., Christen, M., Will, G.: Detection of a flow induced magnetic field eigenmode in the riga dynamo facility. Phys. Rev. Lett. **88**, 3024–3027 (2001)
20. Müller, U., Stieglitz, R.: The Karlsruhe dynamo experiment. Nonlinear Process. Geophys. **9**, 165–170 (2002)
21. Benzi, R., Ciliberto, S., Tripiccione, R., Baudet, C., Massoaioli, F., Succi, S.: Extended self-similarity in turbulent flows. Phys. Rev. E **48**(1), R29–R32 (1993)